Hindawi Publishing Corporation
International Journal of Antennas and Propagation
Volume 2013, Article ID 637270, 16 pages
http://dx.doi.org/10.1155/2013/637270

Review Article

Metamaterial Sensors

Jing Jing Yang,[1] Ming Huang,[1] Hao Tang,[2] Jia Zeng,[1] and Ling Dong[1]

[1] *Wireless Innovation Lab, School of Information Science and Engineering, Yunnan University, Kunming, Yunnan 650091, China*
[2] *Radio Monitoring Center of Yunnan, Kunming, Yunnan 650228, China*

Correspondence should be addressed to Ming Huang; huangming@ynu.edu.cn

Received 5 October 2012; Revised 11 December 2012; Accepted 15 December 2012

Academic Editor: James R. Kelly

Metamaterials have attracted a great deal of attention due to their intriguing properties, as well as the large potential applications for designing functional devices. In this paper, we review the current status of metamaterial sensors, with an emphasis on the evanescent wave amplification and the accompanying local field enhancement characteristics. Examples of the sensors are given to illustrate the principle and the performance of the metamaterial sensor. The paper concludes with an optimistic outlook regarding the future of metamaterial sensor.

1. Introduction

Metamaterials are manmade media with all sorts of unusual functionalities that can be achieved by artificial structuring smaller than the length scale of the external stimulus [1]. They have provided many possibilities for exploring unknown physical phenomena such as reverse Vavilov-Cherenkov effect [2], negative refraction [3], cloaking [4–7], concentrator [8], perfect lens [9], and negative compressibility [10]. In recent years, sensing applications of metamaterials have attracted a great deal of attentions. It is well known that conventional optics suffer from Abbe diffraction limit, since they are only capable of transmitting the propagating components, and the maximum resolution in the image can never be greater than half a wavelength. In a pioneer work, Pendry [9] demonstrated that phase of propagating waves and the amplitude of the evanescent states could be restored by the perfect lens made up of materials with negative index of refraction and thus giving rise to a resolution below the diffraction limit. The essence of the perfect lens lies in the evanescent wave amplification induced by the negative refraction materials. It has been achieved experimentally by Grbic and Eleftheriades [11] using transmission line metamaterials. For the metamaterial slab with thickness of d and loss of δ, the resolution will be $\Delta = 2\pi d/\ln(2/\delta)$ [12]. If the loss approximated zero, infinite resolution could be realized. Although the loss metamaterials cannot be eliminated, and perfect lens does not change the decaying character of evanescent wave, the idea of far field perfect imaging through converting evanescent waves to propagating waves has been proposed and demonstrated experimentally [13, 14]. On the other hand, the amplification of evanescent wave has been shown to be able to enhance the interaction between wave and mater and then increase the sensitivity of sensors [15]. A large number of researches about metamaterial sensors have emerged over the last several years. Schueler et al. [16] reviewed the metamaterial inspired composite right/left-handed transmission line microwave sensors. Chen et al. [17] reviewed metamaterials application in sensing with an emphasis on split ring resonator-based sensors. Our group has been dedicated to the study of metamaterial sensors for a long time, and a great portion of works have been done [15, 18–29]. Zheludev [30] analyzed the future development of metamaterials and pointed out that sensing application represents a growing area.

In this paper, we make a review of the metamaterial sensors with an emphasis on evanescent wave amplification and the concomitant effects. In Section 2, the generation of surface wave at the boundary between negative and positive materials is revisited, and examples of metamaterial planar waveguide sensors and surface whispering gallery mode sensors are given to illustrate phenomenon of evanescent wave amplification for sensing application. In Section 3, sensors

based on planar metamaterial arrays with enhanced sensitivity for the detection of mechanical deformation, graphene atomic layer, and for label-free image of biochemical samples are introduced. In Section 4, examples of sensors based on stacked metamaterial structures are given to illustrate the subwavelength imaging characteristic. Section 5 focuses on the metamaterial sensors based on a single metamaterial particle with the advantages of fabrication simplicity and experimental robustness. In Section 6, the other kinds of metamaterial sensors such as the sensors based on squeezing and tuning effect of epsilon near zero materials and the open cavity are illustrated. In the last section, a conclusion is given.

2. Evanescent Wave Amplification

In 2000, Pendry [9] found that negative refraction makes a perfect lens due to the amplification phenomenon of evanescent wave. To give a vivid picture of this phenomenon, we revisit the slab waveguide model shown in Figure 1(a). In the case of time harmonic field and lossless, that is, both ε and μ are all real numbers, suppose that magnetic field H is polarized along the y-axis and TM wave travels in the z-direction. When a layer of metamaterials is covered on the surface of the guiding layer as shown in Figure 1(b), evanescent wave at the boundary between the metamaterial layer and the cladding layer will be amplified. This can be proved by deriving the dispersion equation of this structure. Figure 2 shows the distribution of $H_y(x)$ along the x-axis of the simulation model. It can be seen that the evanescent wave in cladding layer is enhanced by metamaterial layer [15].

2.1. Planar Waveguide Sensor. Waveguide sensors have found a wide range of applications such as the detection of harmful gases [31] and chemical analytes [32]. Such sensors are also known as evanescent wave sensors because of the evanescent wave entering into the analyte whose refractive index is to be measured. Due to the interaction of the analyte and the evanescent wave, changes can be observed in the absorption or phase shift of the light propagating through the waveguide, giving an indication of the concentration of refractive index of the analyte. The amplification of evanescent wave forms the basis for increasing the sensitivity. Many researchers have attempted to increase the penetration depth and strength of evanescent wave by bending or tapering the optical fiber [33–37] and altering the light launching angle [38]. Horváth et al. [39, 40] have shown that penetration depth of evanescent wave can be increased by using reverse symmetry configuration that the refractive index of the aqueous cladding is higher than that of the substrate material. Taya et al. [41] investigated the sensitivity of asymmetrical optical waveguides with nonlinear cladding and substrate, of which the permittivity displays a Kerr-type response. They show that sensitivity of the nonlinear planar asymmetrical optical waveguide sensor is higher than that of the conventional asymmetrical optical waveguide sensor. Through inserting a layer of metamaterials with negative permittivity and negative permeability between the cladding and the guiding layer, they found that the sensitivity of the waveguide sensor can be dramatically enhanced [42]. We [18] studied the

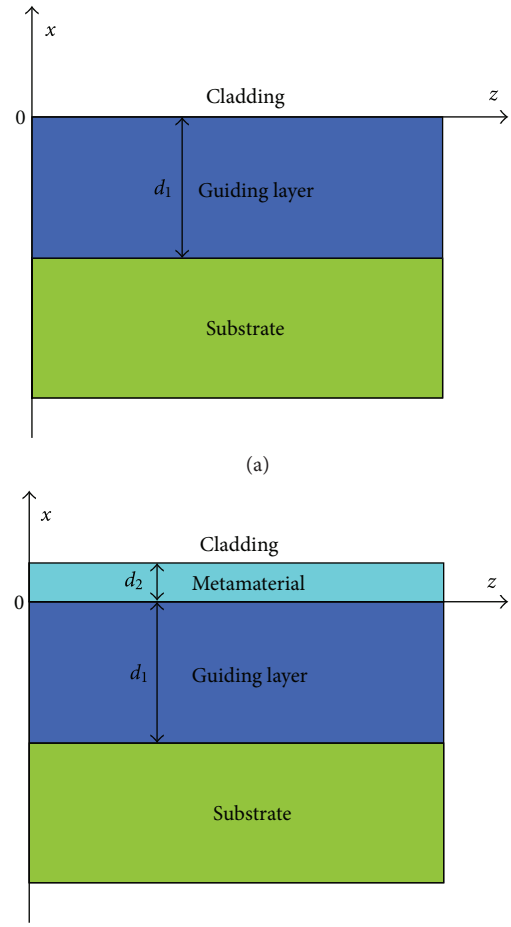

Figure 1: Simulation model of the traditional planar waveguide sensor (a) and the planar waveguide sensor covered with a layer of metamaterials (b).

dispersion equation of TM mode planar optical waveguide with metamaterial layer and showed that the sensitivity of this waveguide was much higher than that of traditional TM mode planar optical waveguide sensor. Recently, the nonlinear planar optical waveguide sensor with metamaterial layer is proposed by our group [19, 20], and both the TE and TM mode dispersion equations are derived and analyzed in detail. We demonstrated that metamaterials combined with nonlinear waveguide will further enhance the sensitivity of the optical waveguide sensors.

Figure 3(a) shows the schematic diagram of a four-layered waveguide sensor model. It is supposed to be infinite in both the z- and y-direction. The waveguide consists of four layers, from the top to the bottom, which are semi-infinite nonlinear cladding, metamaterial layer, guiding layer, and semi-infinite nonlinear substrate, respectively. Thickness of the guiding layer and the metamaterial layer is denoted as d_1 and d_2, respectively. Permittivities of the four layers are ε_{nlc}, ε_m, ε_g, and ε_{nls}. The TM mode nonlinear cladding and substrate are supposed to be Kerr type. Normalized magnetic fields of the nonlinear planar waveguide sensor with and without the metamaterial layer are simulated and compared in

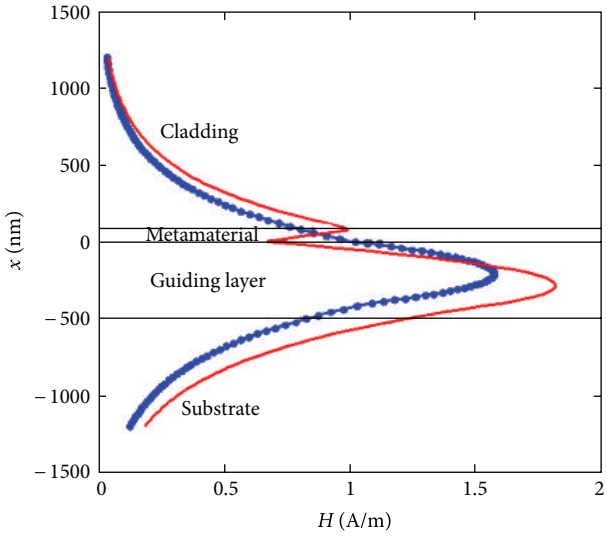

FIGURE 2: Magnetic field $H_y(x)$ distribution in the conventional planar waveguide sensor (blue dotted line) and metamaterials assisted planar waveguide sensor (red line), and d_2 is the thickness of the metamaterials (red line) [15].

Figure 3(b). We can clearly observe that there is a sharp increase of evanescent field at the boundary between the metamaterial layer and the nonlinear cladding. The magnetic field intensity at the surface of the metamaterial layer is about 2.46 times that of the waveguide without the metamaterial layer. For the TE mode nonlinear planar waveguide, the evanescent application phenomenon can also be obtained.

Sensitivity (S_m) of the sensor depends on the modal effective index (N) change rate with respect to the change of cladding index (n_c), that is, $S_m = (\partial N/\partial n_c)$. Through differentiating the dispersion relation of the nonlinear planar waveguide sensor, the sensitivity can be obtained. Sensitivity versus d_1 for the nonlinear optical waveguide sensor with metamaterials (S_m) and without metamaterials (S_{nm}) is plotted in Figures 4(a) and 4(b). In the case of normal symmetry ($a_s > a_c$), sensitivity increases with guiding layer thickness and reaches a maximum value at a point around $d_1 = 200$ nm and then decreases gradually. Here, $a_s = \varepsilon_s/\varepsilon_g$ and $a_c = \varepsilon_c/\varepsilon_g$ are the asymmetry parameters. In the case of reverse symmetry ($a_s < a_c$), the sensitivity decreases monotonously with d_1. Comparing the two figures, we can conclude that metamaterials can improve the sensitivity of the optical waveguide sensor, and the optical waveguide sensors with metamaterials in reverse symmetry mode has much higher sensitivity. For TM and TE mode optical waveguide sensors with metamaterials, the sensitivity as a function of d_1 is simulated and shown in Figures 4(c) and 4(d). In the case of normal symmetry shown in Figure 4(c), an optimal guiding layer thickness is observed at around 60 nm for TE mode, while the optimal guiding layer thickness for TM mode sensor is about 220 nm. In the case of reverse symmetry shown in Figure 4(d), sensitivity decreases gradually with d_1, and the thinner the guiding layer, the better the performance of the sensor. Therefore, the sensitivity of TM waveguide sensor in reverse symmetry configuration possesses much higher sensitivity than TE waveguide sensor.

2.2. Surface Whispering Gallery Mode. From the previous analysis, we can conclude that the sensitivity of the planar waveguide sensor can be greatly enhanced by metamaterials due to the amplification of evanescent wave. Interestingly, we find that when the dielectric slab covered with a layer of metamaterials with negative permittivity and/or permeability is bent over to form a four-layer cylindrical waveguide as shown in Figure 5(a), the evanescent wave can also be amplified [21]. Figure 5(b) shows the cross-section of the cylindrical waveguide structure. Electric field distribution in the cross-section of the dielectric waveguide coated with a layer of metamaterials at the eigenfrequency of $f_e = 165.664$ THz is plotted in Figure 5(c). Figure 5(d) displays the electric field distribution in the cross-section of a conventional dielectric waveguide. It is clear that for the metamaterial-assisted microring, maximum electric field of WGM moves to the surface of the metamaterial layer. This is named as surface whispering gallery mode (SWGM). It exposes a strong evanescent field to the surrounding, and thus this region will be quite sensitive in dielectric environment. Besides, SWGM can also be generated on the inner surface of a hollow dielectric waveguide and the surface of a circular or elliptical dielectric cylinder when coated with a metamaterial layer [22–24].

The SWGM sensor has been demonstrated to have much higher sensitivity than that of conventional WGM sensor. To give a quantitative illustration for the sensitivity of the SWGM sensor, resonant frequency, frequency shift, and Q factor of the SWGM in dielectric sensing are simulated and compared with the traditional WGM sensor, as shown in Table 1 [21]. For the WGM sensor, the average frequency shift to an increase of 0.02 in substance permittivity is only 13.25 GHz, and the sensitivity (defined as resonance wavelength shift over the refractive index change unit) is about 1.4 nm/RIU. For the SWGM sensor, the response to an increase of 0.02 in substance permittivity is a significant resonant frequency downshift of 187 GHz in average, and the sensitivity is about 29 nm/RIU, which is more than 20 times that of the WGM sensor. This is due to the amplification of evanescent field which ensures a strong interaction between light and substance. Interestingly, the sensitivity of the SWGM sensor can be further enhanced by increasing the thickness of the metamaterial layer. Figure 6 shows the relation between resonant frequency and substance permittivity for different metamaterial layer thickness (t). When the thickness of metamaterial layer is 0.05 μm, the average frequency shift in response to a 0.02 increase in substance permittivity is about 42 GHz, and the sensitivity is 5 nm/RIU. When the thickness of metamaterial layer is 0.2 μm, the average frequency shift will be 204 GHz, and the sensitivity can be increased up to 50 nm/RIU. This is because much more power is transferred to SWGM with increasing metamaterial thickness. Recently, we have demonstrated theoretically that when a layer of Au film is deposited on the microring instead

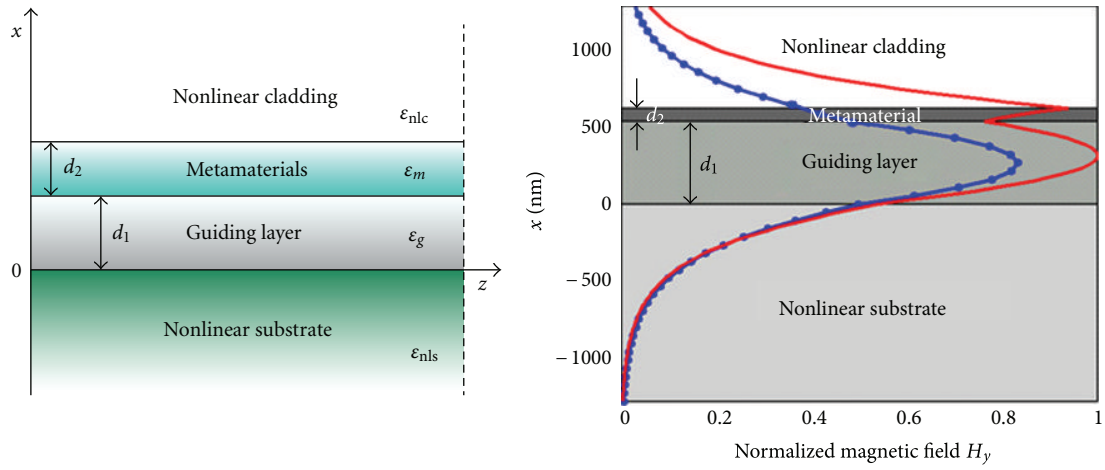

FIGURE 3: (a) Schematic diagram of a cross-sectional view of the nonlinear planar waveguide sensor with a metamaterial layer. $d_1 = 500$ nm, $\varepsilon_c = 2$, $\varepsilon_s = 2.2$, $\varepsilon_g = 4$, $\varepsilon_m = -2$, $d_2 = 80$ nm, $n = -0.6$, and $\lambda = 1550$ nm. (b) Normalized magnetic field H_y distribution along the x-direction of the nonlinear planar waveguide sensor without (dotted blue line) and with the metamaterial layer (solid red line) [20].

TABLE 1: Q factor, resonant frequency, and frequency shift of WGM sensor and SWGM sensor [21].

Sensor		ε_s 1.02	1.04	1.06	1.08	1.1
WGM	Q	15718	15661	15777	15718	15658
	f_r (THz)	198.248	198.235	198.221	198.208	198.195
	Δf_r (GHz)	13	14	13	13	
SWGM	Q	16930	16922	16923	17083	17072
	f_r (THz)	165.474	165.286	165.097	164.911	164.725
	Δf_r (GHz)	188	189	186	186	

of the metamaterial layer, SWGM can also be excited when the excitation frequency is lower than plasma frequency [45].

3. Planar Metamaterial Array

Planar metamaterials consisting of subwavelength resonators have been proposed for thin dielectric film sensing. To achieve higher sensitivity, the sensor needs to have a sharp resonance in its frequency response and a high concentration of electric field to enable the detection of small changes in dielectric environment. When analyte is deposited on the surface of the resonators, the effective permittivity at the gap of each resonator is increased. Then, the gap undergoes a significant change in the charge distribution and capacitance, which can be observed from the transmission resonance. This sensing mechanism has been demonstrated experimentally and successfully applied to a range of planar metamaterial sensors [43, 44, 46–51]. For example, Melik et al. [48] demonstrated that the metamaterial-based strain sensors are highly sensitive to mechanical deformation, due to the large transmission dips and high quality factors. The detection of a single atomic layer of graphene was realized by Papasimakis et al. [49] based on the metamaterial sensor made up of an array of asymmetrically split ring resonators. Liu et al. [51] showed that the metamaterial sensor fabricated using gold film may serve as a highly efficient localized surface plasmon resonance sensor in the near-infrared with sensitivity of 588 nm/RIU.

An intracellular plasmonic label-free imaging by exciting multimode resonances in spilt-ring resonators is proposed by Lai et al. [43]. Figure 7 shows the SEM images of the designed SRR samples which were fabricated by standard e-beam lithographic and lift-off processes. One sample contains 10 × 10 unit cells, and each unit cell consists of 5 × 5 SRRs. All SRR unit cells contain exactly identical SRR pattern from cell to cell. To demonstrate the performance of the planar metamaterial sensor, bioimage of human bone marrow-derived mesenchymal stem cells (hMSCs) based on the fundamental resonance signal of SRR at the wavenumber of 1850–2400 cm^{-1} was conducted and compared with conventional imaging technology. Figure 8(a) shows the conventional optical microscopic image of the hMSCs grown on the SRRs samples. The black part in the background refers to the SRRs structure. In this case, any detail of the inner nucleus and organelles cannot be revealed without the labeling process. Figure 8(b) shows the confocal fluorescent optical microscopic image of the hMSCs, in which the nuclei of the hMSCs can be observed. However, such a labeling process is typically expensive and time consuming, impeding the practical application of real-time diagnosis. Figure 8(c) displays the intracellular image of the hMSCs by the SRR platform. It does not require the labeling process but directly detects the change of plasmonic resonance of the SRR fluctuated by the local attachment of the targeting bioagents. In the experiment, transmission and reflection were characterized by a Fourier-transform infrared spectrometer equipped with an infrared microscope in the wavenumber range of 400–8600 cm^{-1}, and the corresponding mid-IR

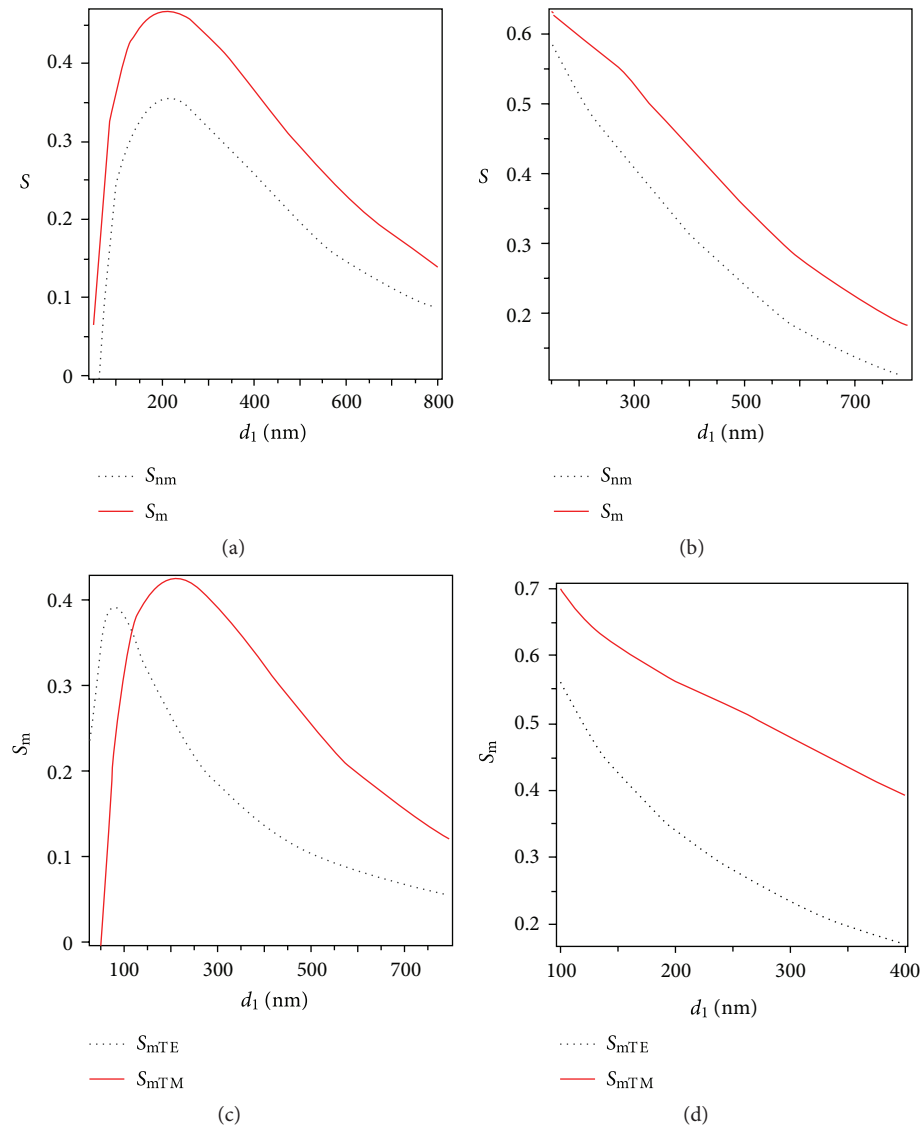

FIGURE 4: Sensitivity versus the guiding layer thickness d_1 for the proposed sensor ($a_m = \varepsilon_m/\varepsilon_g = -0.5$, $n = -0.6$, and $d_2 = 30$ nm) with a metamaterial layer (red solid line) and without a metamaterial layer (blue dotted line): (a) normal symmetry ($a_s = 0.55$ and $a_c = 0.5$) and (b) reverse symmetry ($a_s = 0.5$ and $a_c = 0.55$). Sensitivity versus the guiding layer thickness d_1 for TM mode (S_{mTM}) (red solid line) and TE mode (S_{mTE}) (blue dotted line) ($d_2 = 20$ nm, $a_m = \varepsilon_m/\varepsilon_g = -0.5$, and $n = -0.6$): (c) normal symmetry ($a_s = 0.55$ and $a_c = 0.5$) and (d) reverse symmetry ($a_s = 0.5$ and $a_c = 0.55$) [20].

images were captured by a focal planar array detector. All measured spectra have been normalized with respect to the reflection spectra of an aluminum mirror. In Figure 8(c), the region colored in red represents the nucleus. This is corresponding to the greatest shift of Resonant frequencies and the strongest reflection intensity. The other colored parts mainly refer to the cytoplasm, corresponding to the smaller shift of resonant frequencies. In short, this study demonstrated the feasibility of using SRRs for constructing the refractive index distribution of hMSCs to obtain images of the target cells. The SRR platform possesses many advantages beyond other optical microscopy such as label-free and real-time diagnosis.

A metamaterial-based terahertz (THz) sensor for thickness measurements of subwavelength thin materials and refractometry of liquids is proposed by Reinhard et al. [44]. The sensor operates in reflection geometry and exhibits a strong frequency shift of a sharp Fano-type resonance minimum in the presence of a dielectric sample. The magnitude of this shift depends on both the refractive index and the thickness of the sample. The unit cell is a square with an edge length of 140 μm, consisting of four metallic crosses on top of a 10 μm thick dielectric matrix with a relative permittivity $\varepsilon_r = 2.67$. Each of the crosses is titled by an angle of 22.5°. Details about the geometry parameters are shown in Figure 9(a). When excited by a horizontally polarized THz wave, the distribution of currents and charge is shown in Figure 9(b). Figure 9(c) is a microscope image of the fabricated metamaterials. In order to experimentally prove the capability of the sensor of measuring the thickness of thin

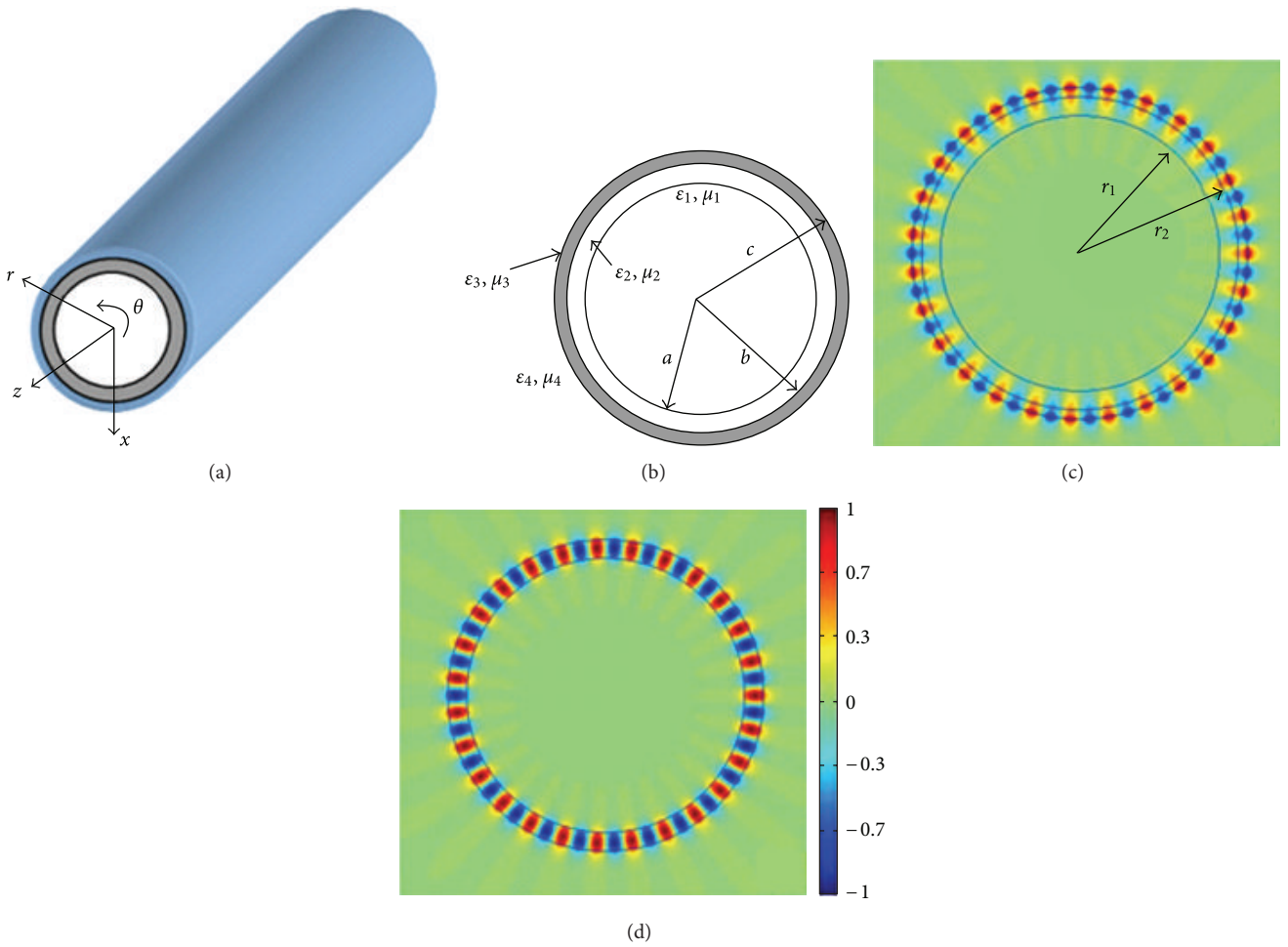

Figure 5: (a) Cylindrical dielectric waveguide covered with a layer of metamaterials. (b) Cross-section of (a). Analytical results of normalized electric field distribution (mode 27) in the cross-section of the waveguide with (c) and without the metamaterial layer (d) [21].

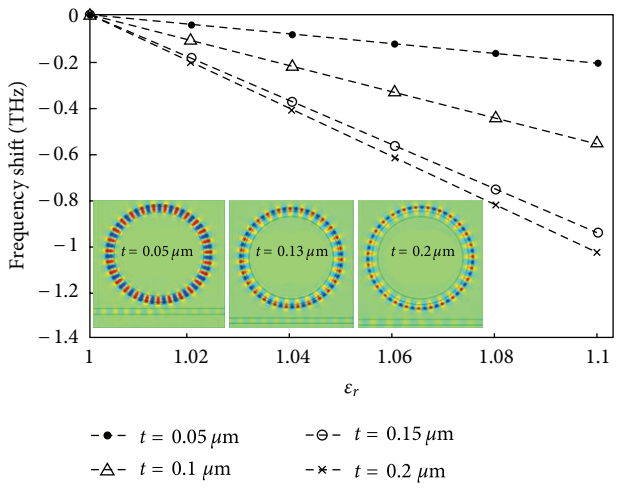

Figure 6: The relation between ε_r and resonant frequency for different metamaterial layer thickness. The insets show electric field distributions at resonant state for $t = 0.05\,\mu$m, $0.12\,\mu$m, and $0.2\,\mu$m, respectively [21].

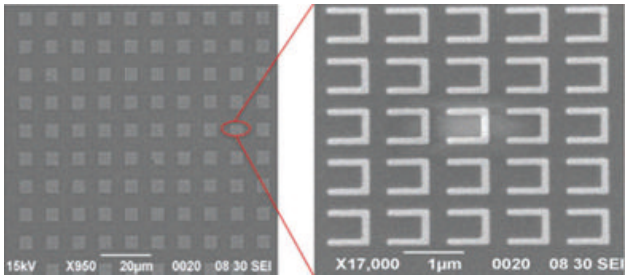

Figure 7: The SEM images of the fabricated planar SRRs. The sample consists of 5 × 5 SRRs as a unit cell through standard e-beam lithographic and lift-off processes [43].

sample materials, silicon layers ($n = 3.4$) with thicknesses between approximately 50 nm and $1\,\mu$m were evaporated on top of the metamaterial sensor, and the reflection spectra were measured using THz time-domain spectroscopy. Figure 10(a) shows the variation of the Resonant frequency of the sensor as a function of silicon thicknesses. The sensitivity of the sensor has a maximum value of approximately

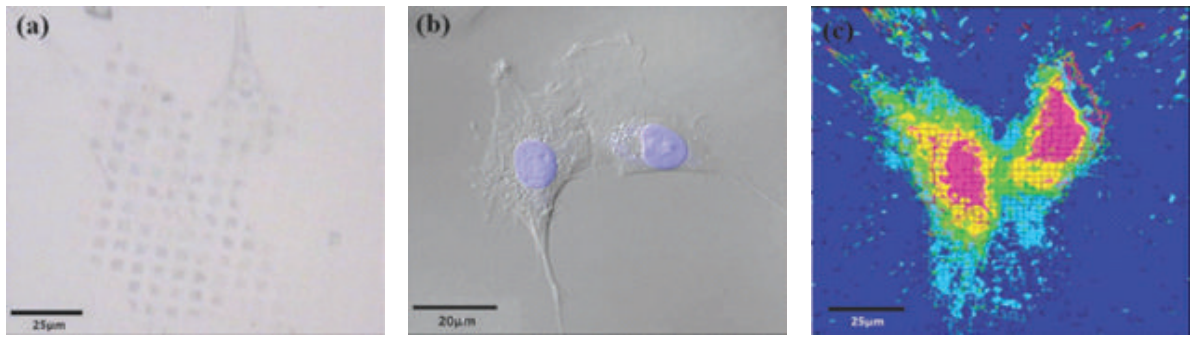

(a) (b) (c)

Figure 8: (a) The unlabeled optical microscopic image of hMSCs on the SRR substrate. (b) The confocal fluorescent microscopic image of the hMSCs. (c) The intracellular image of the hMSCs by the SRR platform [43].

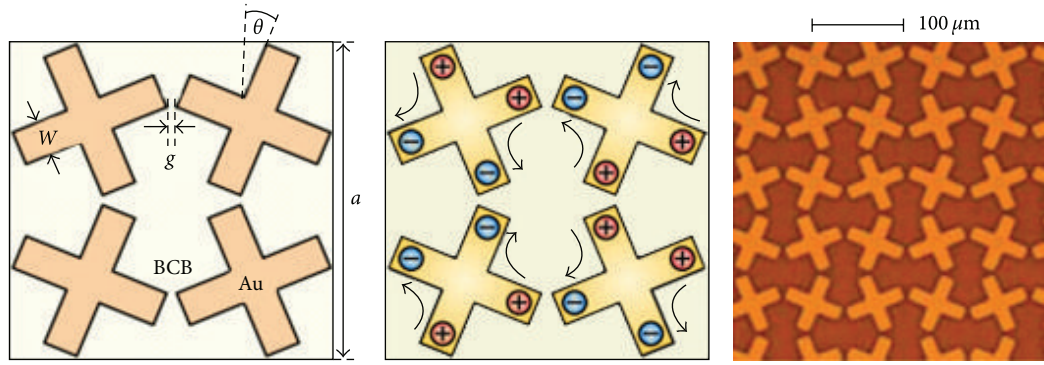

Figure 9: Geometry parameters of the metamaterial unit cell. $a = 140\,\mu$m, $w = 15\,\mu$m, $g = 4\,\mu$m, and $\theta = 22.5^{\circ}$. The metamaterial consists of gold (Au) crosses on top of a BCB film. (b) Distribution of charges (+, −) and currents (arrows) at resonance when excited by a horizontally polarized incident THz wave. (c) Microscope image of a fabricated metamaterials [44].

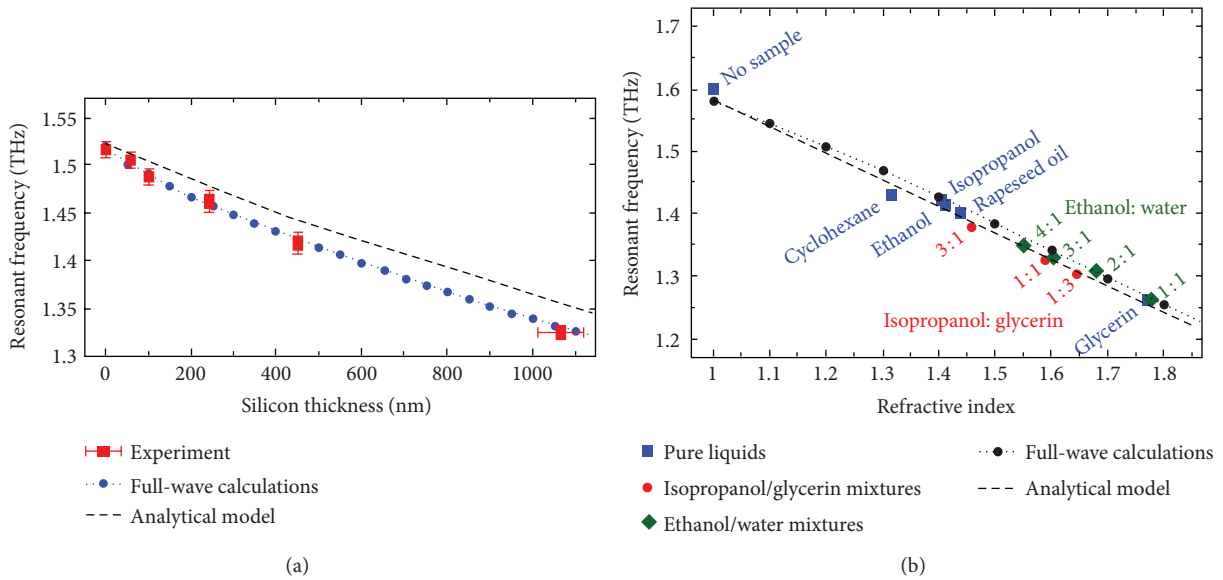

Figure 10: (a) Resonant frequencies of the sensor in dependence on silicon thickness. The slope of the curve has a maximum value of 0.4 THz/μm. (b) Experimentally measured Resonant frequencies of the metamaterial sensor in the presence of several liquids and liquid mixtures [44].

0.4 THz/μm for very small layer thickness, and the thickness resolution is 12.5 nm, which corresponds to approximately 1/16000 of the THz wavelength. To demonstrate the effectiveness of the metamaterial structure as a liquid sensor, resonant frequencies in the presence of different liquid sample substances are measured as shown in Figure 10(b). The refractive index sensitivity is 0.43 THz per refractive index unit.

In the previous cases, the sample substances that deposited on the surface of the metamaterial give rise to a shift in resonant frequency due to the change of capacitance. In a recent work, Kenanakis et al. [46] studied the sensing capability of a metamaterial structure made of a pair of square metal slabs as shown in Figure 11. The whole structure contains 10×10 unit cells. Each side of the pair is printed on a separate FR-4 boards placed facing each other at a distance d, with the printed metallic structures facing outwards. The space of thickness d between the two FR-4 boards is filled (or partially filled) with the materials of interest. To demonstrate the sensing capacity of the metamaterial structure, transmission spectrum for air, low density polyethylene (LPDE), FR-4, and p-type silicon are measured and compared with numerical simulation, as shown in Figure 12. Aside from the very good agreement between simulations and experiments, we can observe in Figure 12 a quite large shift of the magnetic resonance to lower frequencies as the permittivity of the dielectric between the slab pair changes from 1.0 (air) to 11.90 (silicon). Besides, the metamaterial structure is also applicable for measuring the thickness of thin dielectric layer placed between the slabs of the pairs. The experimental results show that a very thin layer of LDPE with thickness of 0.1 mm can lead to a Resonant frequency shift as large as 0.5 GHz, indicating the large sensitivity of the design.

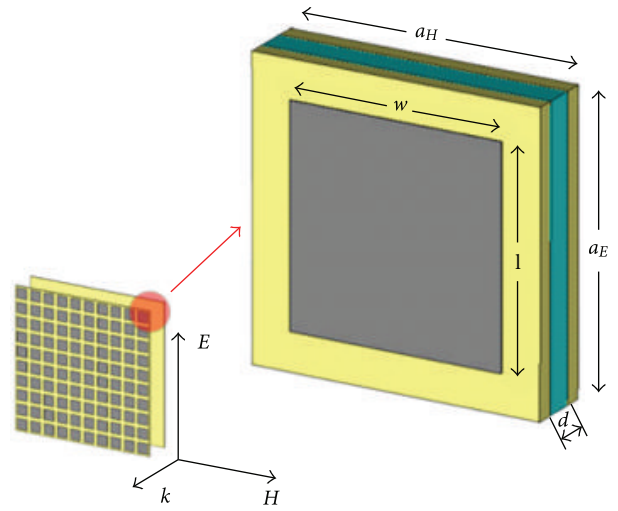

Figure 11: Schematic of the slab pair structure. A magnification of one unit cell of the slab pair structure (red shadowed area) is presented. E, H, and k correspond to electric field, magnetic field, and the wave vector, respectively [46].

4. Stacked Metamaterial Structure

Unit cells of metamaterials are usually stacked together to make novel electromagnetic devices [1, 37–39]. Besides, it has been demonstrated that the stack of metamaterial particles or particle arrays is capable of increasing the interaction between wave and matter and then enhancing the sensitivity of sensors [52]. Liu et al. [53] experimentally demonstrated a nanoplasmonic analogue of electromagnetically induced transparency using a stacked optical metamaterials. Results show that plasmonic structures enable large field strengths within small mode volumes, and this may pave the way towards ultracompact sensors with extremely high sensitivity. Seo et al. [54] reported the experimental observations of trapped mode resonances in stacked symmetric electric ring resonators separated by dielectric inserts. This opens an alternative way of forming sharp resonances in a symmetric metamaterial structure which may have potential applications in sensor design. Han et al. [55] studied the transmission properties of stacked SRR arrays, and sharp resonance coupled with field concentration phenomenon, which satisfy the requirement of an effective senor were observed. Aylo et al. [56] investigated the transmission and reflection spectra of periodic and random stacks comprising positive index materials and negative index metamaterials based on transfer matrix method, and the effectiveness of this structure as a pressure sensor was demonstrated.

On the other hand, the stack of metamaterial structures has been demonstrated to be able to realize perfect lens and to enhance the resolution of sensors [57, 60–63]. For example, an impedance-matched, low loss negative index metamaterial superlens was reported by Aydin et al. [62]. It is capable of resolving subwavelength features of a point source with a 0.13 wavelength resolution. Yang et al. [63]. studied the potential of quantum metamaterial for subwavelength imaging applications in the mid-infrared. FDTD numerical simulations demonstrated the negative refraction along an air/metamaterial interface, and a sub-diffraction-limited image of a structure that is ten times smaller than the incident wavelength. A novel microwave nondestructive evaluation sensor based on a negative index material lens constituted of stacked SRR structures for detection of material defects was proposed and fabricated by Shreiber et al. [57]. A sketch of the sensor system is illustrated in Figure 13(a). The lens is made up of a stack of double split resonators. Simulation models of the 1D and 2D lenses are shown in Figures 13(b) and 13(c). The author investigated the performance of the metamaterial lenses for the detection of material defects which were small relative to wavelength. In the sensor system, the sample is positioned at the focus spot of the lens. The defect in the sample will induce some significant changes in the energy density detected by the monopole. Ideally, the same monopole could be used to detect the reflected signal, but because the metamaterial is lossy, an additional monopole was placed on the other side of the lens to detect the reflected signal from the sample. Experimental results show that both the 1D and 2D lenses are capable of detecting a 3 mm (0.037 λ) diameter through a hole in a fiberglass material sample based on analyzing the receiving power of the monopole, but the image obtained with the 2D lens is much sharper. Figure 14 shows a comparison of the focusing spot size obtained for the

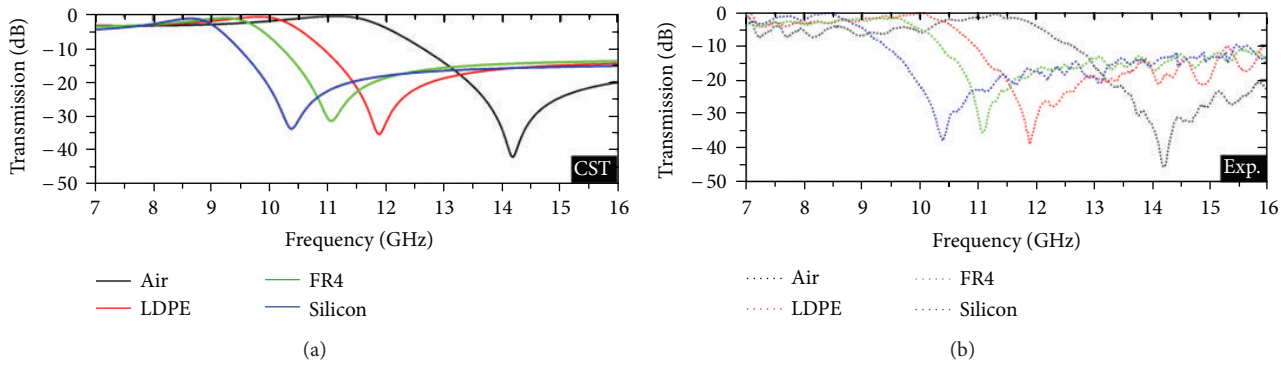

FIGURE 12: Simulation ((a) solid lines) and experimental results ((b) dotted lines) regarding the transmission of the slab pair structure enclosing several materials with a thickness of 0.5 mm [46].

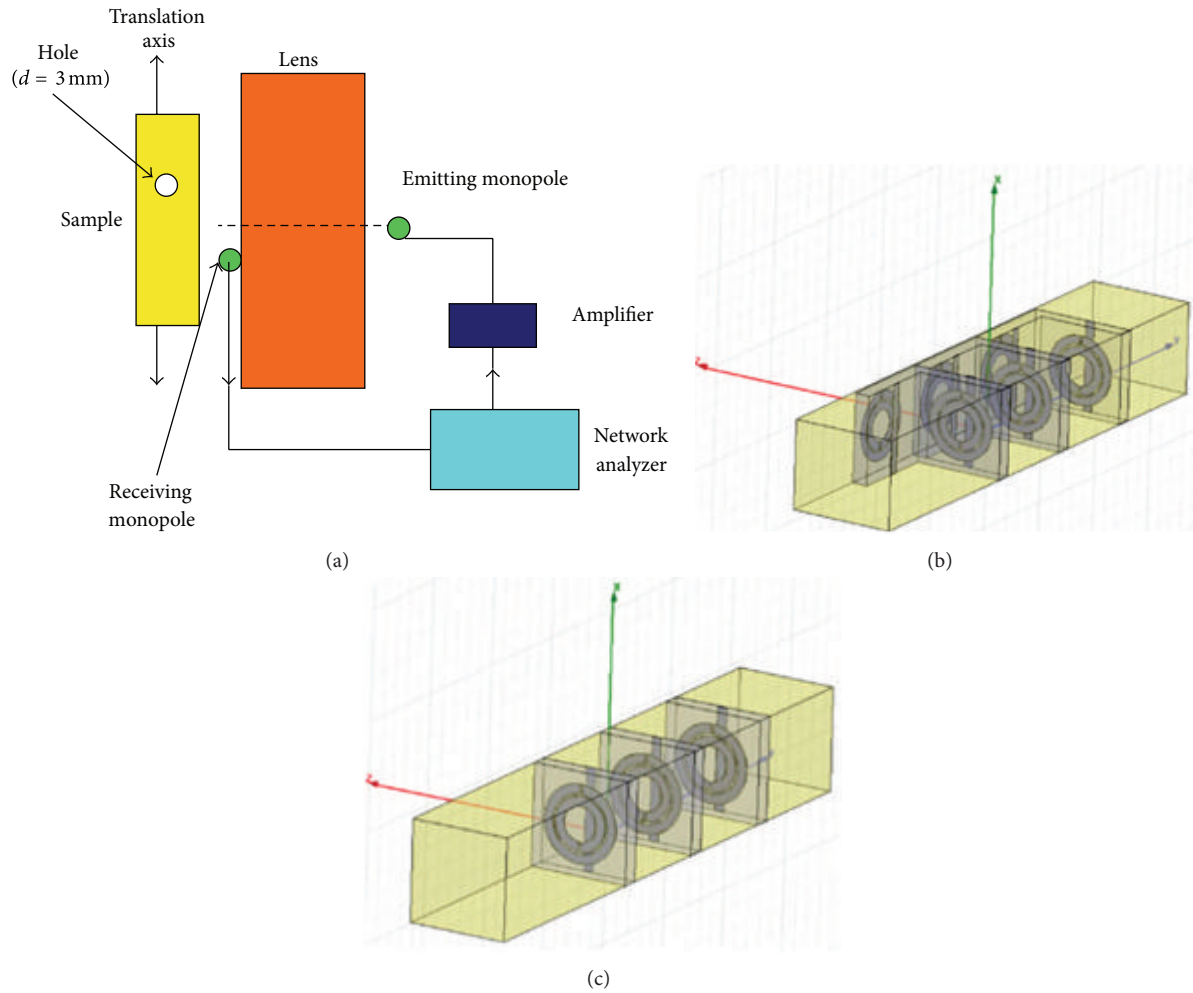

FIGURE 13: (a) Sketch of the nondestructive evaluation sensor system. (b) 2D unit cell models. (c) 1D unit cell models [57].

1D and 2D lenses. The 1D lens yielded a focus spot size of 0.7 λ, whereas the focus spot for the 2D lens is about 0.48 λ. On the other hand, due to the influence of metamaterial loss, the transmittance of the 2D lens is much lower than that of the 1D one, and then the 1D lens allows for a longer sample standoff distance and higher transmission. Therefore, the choice of the lens to be used in a sensor is prescribed by the specific requirements of the testing system.

5. Sensors Based on a Single Metamaterial Particle

In a pioneering work, Fedotov et al. [64] demonstrated that the "trapped mode" resonances could be excited by crossing the symmetry of double split resonators. Metamaterials of this type are known to show Fano antisymmetric resonant lines in transmission with enhanced local fields that appear

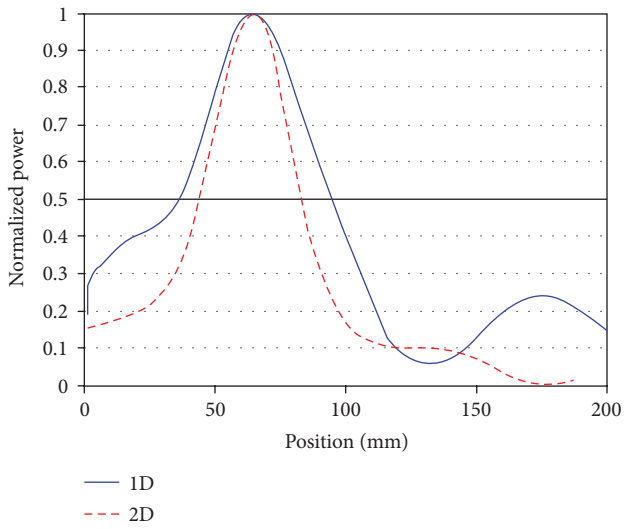

FIGURE 14: Power scans at focus spot distance for 1D lens and 2D lens [57].

"trapped" in the gap of the unit cells. Based on this characteristic, a metamaterial particle-assisted thin film sensor was proposed and demonstrated experimentally by Al-Naib et al. [58]. It consists of a single mode rectangular waveguide and a single asymmetry double split resonator (aDSR), as shown in Figure 15(a). In this device, the excitation of "trapped modes" leads to an extremely sharp resonance. Then, at the resonant state, the electric field concentrates in the gap of the ring (see Figure 15(c)), and this region becomes sensitive in dielectric environment. To evaluate the performance of the sensor, the aDSR was coated with a 17.8 μm thick layer of photoresist in four degrees of coverage, and the transmission coefficient was measured as shown in Figure 16. The circular aDSR features a resonance shift of 9, 24, and 48 MHz for the single-covered square, the two covered squares, and the full coverage, respectively, demonstrating the enhanced sensitivity of the sensor. Since only a single aDSR is required, the design of such a resonant sensor is quite flexible. Besides, the aDSR is located in the waveguide and shielded against environmental influence, so that the measurement is robust and highly reproducible.

Following the work of Al-Naib et al., great efforts have been dedicated to study the sensors based on single metamaterial particles. For example, He et al. [65] proposed and demonstrated the implementation of tip-shaped split ring resonator in microwave thin film sensing. An evanescent microwave probe composed of a single SRR excited by a simple rectangular loop is proposed by Ren et al. [66]. It has the advantages of simple fabrication and low cost. Numerical and experimental results show that the presence of the single SRR enhances the evanescent field concentration in the close proximity of the probe, and then the sensitivity of the probe is improved substantially. Our group [25] reported a double negative material particle-assisted microwave sensor and demonstrated that when a pair of Ω-shaped particles is located in a rectangular waveguide, the transmission can be greatly enhanced, and such a novel sensor possesses much higher sensitivity than that of traditional microwave sensor. Besides, we investigated the influence of shape and asymmetric parameters of the aDSR on the performance of the sensor [26]. Results show that the spectral response and the Q factor of the sensor can be flexibly tailored to design requirements by adjusting the asymmetry parameter or the topological structure of the resonator. Recently, we reported an optimized design concept for a microwave resonant sensor based on stereocomplementary asymmetric split resonator (CASR) [27]. In terms of its special structure characteristic, the stereo-CASR can be perforated on a copper sheet, and thus the influence of the substrate losses on Q factor can be eliminated. Figures 17(a) and 17(b) show the electric field distribution and the corresponding power flow on the surface of the resonator at the resonant state. We supposed that the sample substance was deposited in the low gap of the structure and the spectrum was simulated, as shown in Figure 17(c). It is seen that the spectrum moves to the lower frequency side with the increase of sample permittivity. The average frequency shift with respect to a small change of 0.1 in sample permittivity is about 123 MHz. The relation between resonant frequency and sample permittivity plotted in Figure 17(d) reveals a good linearity of the sensor. Moreover, the simplicity of such sensing structure enables its utilization in a wide frequency range by simple rescaling, which opens up avenues toward flexible designing of sensors with superior sensitivity.

6. The Other Kinds of Metamaterial Sensors

The other kinds of metamaterial sensors include sensors based on the squeezing and tunneling effect, combined right/left-handed metamaterial transmission lines (CRLH) [16], metamaterial probe [67], and open resonator [28]. The CRLH sensor is a popular concept for the microwave region. It utilizes metamaterial transmission line unit cells as building blocks and can be exploited to allow for different sensor applications, such as the measurement of mass flow [68], level [69], permittivity [70], strain [71], and the velocity of granular materials on belt conveyor systems [72]. More details relating to this kind of sensors can be found in the review article of Schueler et al. [16]. The metamaterial probe proposed by Boybay and Ramahi [67] consists of a rectangular waveguide with a layer of single negative or double negative metamaterials covered at one end. Due to the application of evanescent wave, it is capable of sensing the target object such as cracks on aluminum plates with subwavelength resolution. The open resonator was firstly proposed by Notomi [73] based on the ray theory in 2000. It consists of two homogenous double negative metamaterial (DNM) squares in the air. Later, the resonating modes in the open resonator were demonstrated numerically by He et al. [74] using the finite-difference time-domain method. Open resonator has been widely applied in dielectric sensing and laser cavity. Recently, we designed and fabricated a novel open resonator using metamaterial transmission line medium [28]. The open resonance effect which is generated by multiple negative reflections is demonstrated experimentally. Figure 18(a) shows the schematic graph of the open resonator. The two DNM squares are colored in blue. Effective permittivity and permeability of the background double

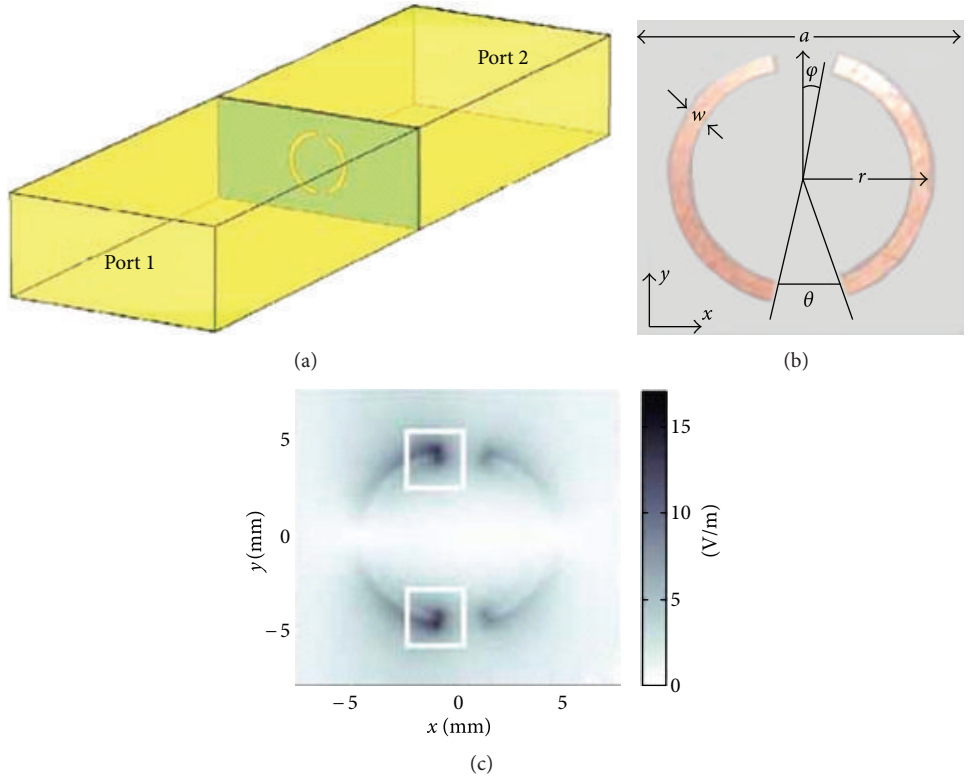

FIGURE 15: (a) Schematic view of the aDSR-assisted sensor. (b) Layout of the circular aDSR. (c) Simulated spatial field distribution for the aDSR [58].

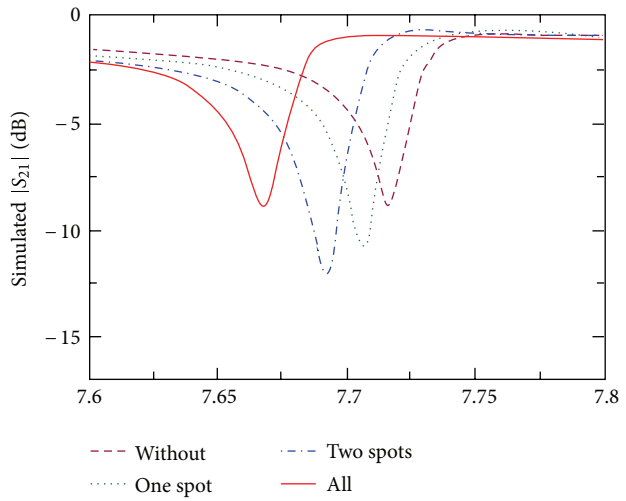

FIGURE 16: Measured transmission response of the aDSR for four degrees of coverage [58].

negative media (DPM) are equivalent to those of the air. A photograph of the open resonator designed based on LC network is depicted in Figure 18(b). The unit cell of the DPM region consists of four surface-mounted inductors in series and one capacitor in shunt to the ground, while the unit cell of the DNM region consists of four surface-mounted capacitors in series and one inductor in shunt to the ground, as shown in the amplified view of Figure 18(b). Simulation results of note voltage distribution obtained based on the software ADS are shown in Figure 18(c). The concentration of voltage at the junction of the DPM square confirms the open resonant characteristic of the structure. Figure 18(d) displays the measurement results of note voltage distribution. Compared with Figure 18(c), the discrepancies are most likely due to tolerances and components losses introduced in fabrication. The field concentration phenomenon observed

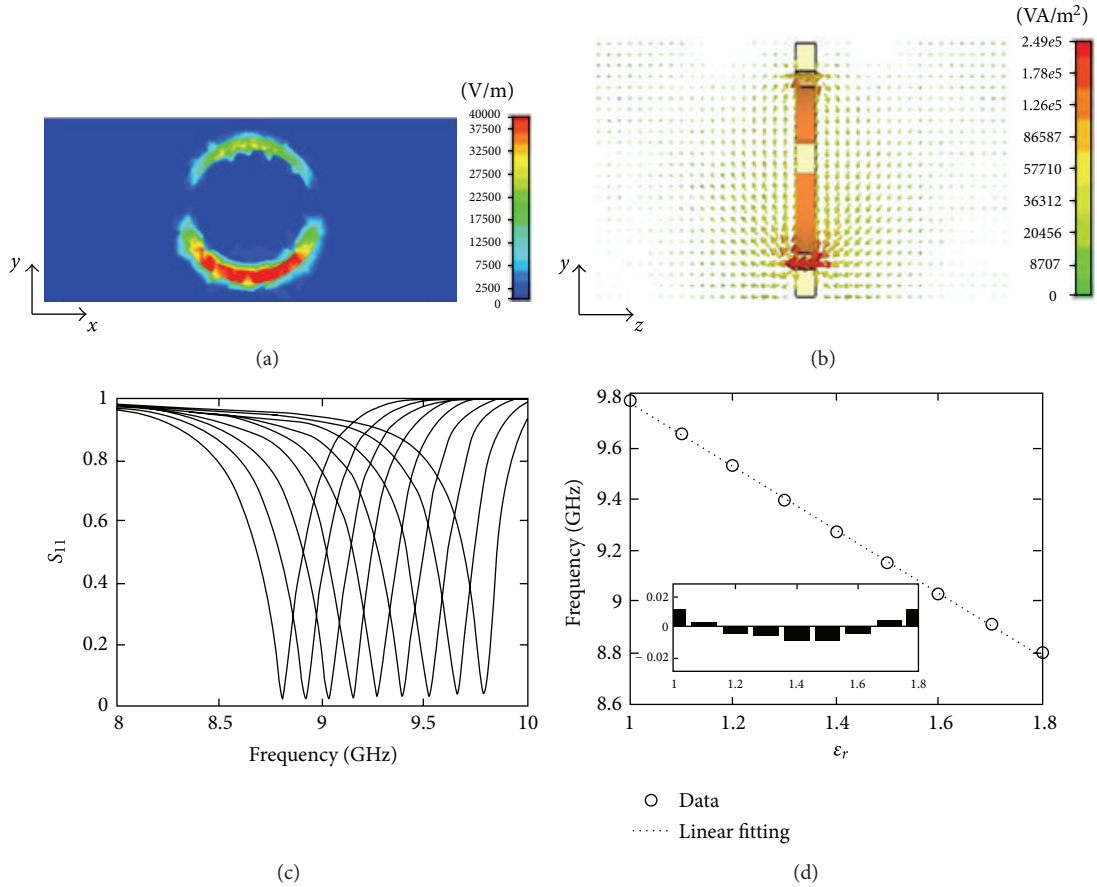

FIGURE 17: (a) Electric field distribution on the surface of the stereo-CASR at resonant state. (b) Corresponding power flow distribution. (c) Reflection spectra of the sensor for a variation of sample permittivity (ε_r). Curves from right to left correspond to $\varepsilon_r = 1$, $\varepsilon_r = 1.1$, $\varepsilon_r = 1.2$, ..., $\varepsilon_r = 1.8$. (d) The relation between resonant frequency and ε_r. The inset shows the residuals of the linear fitting curve [27].

at the resonant state reveals the highquality characteristics of the metamaterial open resonator, which may provide many possibilities for designing sensors with superior performance.

The squeezing and tunneling effect of electromagnetic waves transmission through narrow channels filled with epsilon (ε) near zero (ENZ) metamaterials was demonstrated theoretically by Silveirinha and Engheta [75]. Since the wavelength of radiation inside the ENZ metamaterials is extremely large, waves propagate inside the ENZ material with no relevant reflection losses at abrupt bends or junctions. The theory of energy squeezing and tunneling through an ultranarrow rectangular metallic waveguide was experimentally verified by Edwards et al. [76] using a microwave setup consisting of three distinct regions in a rectangular waveguide with a narrow channel. Alù et al. [59, 77] showed that the phenomenon of energy squeezing and tunneling through a narrow waveguide channel can be used for accurate dielectric sensing application. Figure 19 shows the simulation model of the permittivity sensor, which consists of an ultranarrow rectangular channel connecting the two sections of a waveguide. In this way, the ENZ-related supercoupling effects can be achieved using conventional materials filling in the channel. The infinite phase velocity of the mode near its cutoff results in a uniform and a strongly enhanced electric field along the channel. As a consequence, a small cavity region with permittivity ε_{cav} located in the channel will perturb the tunneling effect clearly and then introduce a significant shift in ENZ-related tunneling frequency. The transmission spectra are shown in Figure 20. From left to right, the curves correspond to the materials with relative permittivity varying from 1 to 2. The peak at about 1.8 GHz is a Fabry-Perot resonance, which is strongly dependent on the length of the channel. Additionally, the squeezing and tunneling effect is independent on the shape of the waveguide. We [29] studied the tunneling of electromagnetic field through a 3D coaxial waveguide channel filled with ENZ materials and showed that the varying of sample permittivity from 1 to 3 will result in a frequency shift of 100 MHz on average.

7. Conclusions

With the development of metamaterial science, sensing application of metamaterials has attracted more and more attention. The amplification of evanescent wave at the boundary between positive and negative refractive index materials not only allows for subwavelength resolution in optical imaging, but also increases the sensitivity of the planar waveguide sensors and the whispering gallery mode sensors due to the

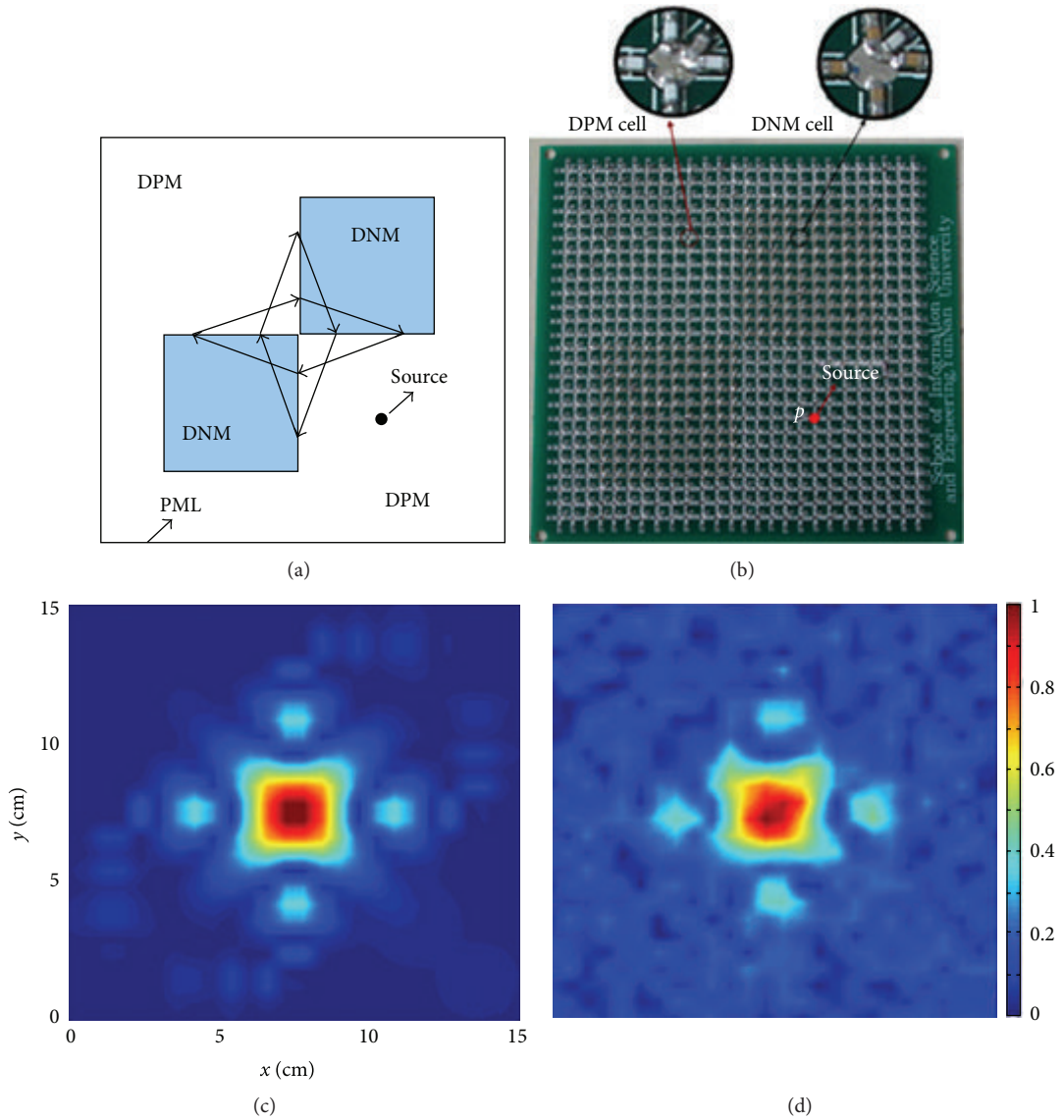

FIGURE 18: (a) Schematic structure of the open resonator consisting of two homogeneous negative refractive index metamaterial squares. (b) Photograph of the metamaterial open resonator based on L-C network. (a) Simulation and (b) measurement results of note voltage distribution [28].

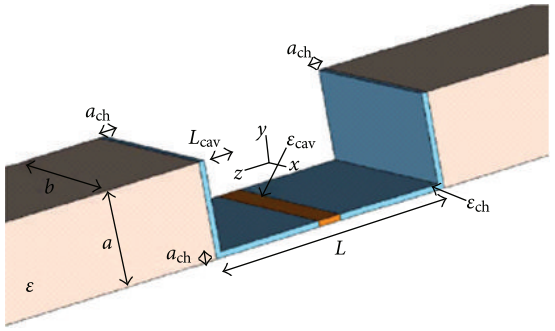

FIGURE 19: Geometry model of the permittivity sensor [59].

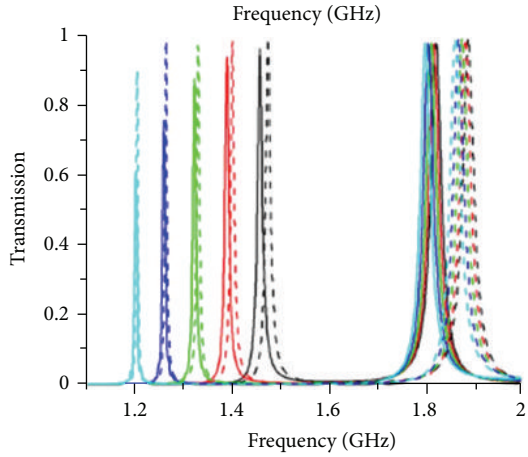

FIGURE 20: Transmission coefficient for the ultranarrow channel sensor with $L = 127$ mm, $b = 2a = 101.6$ mm, $\varepsilon = 2\varepsilon_0$, $\varepsilon_{ch} = \varepsilon_0$, $a_{ch} = a/64$, and $L_{cav} = L/5$ [59].

enhancement of the interaction between wave and matter. Sensors-based metamaterial arrays and particle(s) utilize the local field enhancement and resonant characteristics of metamaterials to achieve high sensitive detection. Besides, simply rescaling the size of metamaterial particles allows for the design of sensors from microwave to optics. Although metamaterial loss cannot be eliminated, reducing the size of metamaterial arrays and using the stereoparticles instead of the planar ones are all effective measures for reducing the impact of losses on sensor performance. We believe that with the development of the research of evanescent wave and the concomitant effects, sensors with excellent sensitivity and subwavelength resolution might be brought by metamaterials in the future.

Acknowledgments

This work was supported by the National Natural Science Foundation of China (Grant nos. 61161007 and 61261002), the Scientific Research Fund Major Project of the Education Bureau of Yunnan Province (Grant no. ZD2011003), the Research Fund for the Doctoral Program of Higher Education (Grant no. 20125301120009), and the Natural Science Foundation of Yunnan Province (Grant no. 2011FB018).

References

[1] N. I. Zheludev, "What diffraction limit," *Nature Materials*, vol. 7, no. 6, pp. 420–422, 2008.

[2] V. G. Veselago, "Electrodynamics of substances with simultaneously negative values of sigma and mu," *Soviet Physics Uspekhi-Ussr*, vol. 10, no. 4, pp. 509–514, 1968.

[3] D. R. Smith and N. Kroll, "Negative refractive index in left-handed materials," *Physical Review Letters*, vol. 85, no. 14, pp. 2933–2936, 2000.

[4] D. Schurig, J. J. Mock, B. J. Justice et al., "Metamaterial electromagnetic cloak at microwave frequencies," *Science*, vol. 314, no. 5801, pp. 977–980, 2006.

[5] S. Guenneau, C. Amra, and D. Veynante, "Transformation thermodynamics: cloaking and concentrating heat flux," *Optics Express*, vol. 20, no. 7, pp. 8207–8218, 2012.

[6] J. J. Yang, M. Huang, C. F. Yang, and J. Yu, "Reciprocal invisibility cloak based on complementary media," *European Physical Journal D*, vol. 61, no. 3, pp. 731–736, 2011.

[7] B. I. Popa, L. Zigoneanu, and S. A. Cummer, "Experimental acoustic ground cloak in air," *Physical Review Letters*, vol. 106, no. 25, Article ID 253901, 2011.

[8] J. Yang, M. Huang, C. Yang, Z. Xiao, and J. Peng, "Metamaterial electromagnetic concentrators with arbitrary geometries," *Optics Express*, vol. 17, no. 22, pp. 19656–19661, 2009.

[9] J. B. Pendry, "Negative refraction makes a perfect lens," *Physical Review Letters*, vol. 85, no. 18, pp. 3966–3969, 2000.

[10] J. N. Grima and R. Caruana-Gauci, "Mechanical metamaterials: materials that push back," *Nature Materials*, vol. 11, no. 7, pp. 565–566, 2012.

[11] A. Grbic and G. V. Eleftheriades, "Overcoming the diffraction limit with a planar left-handed transmission-line lens," *Physical Review Letters*, vol. 92, no. 11, pp. 117403–1, 2004.

[12] R. Marqués, F. Martín, and M. Sorolla, *Metamaterials with Negative Parameters: Theory, Design, and Microwave Applications*, Wiley-Interscience, Hoboken, NJ, USA, 2008.

[13] Z. Jacob, L. V. Alekseyev, and E. Narimanov, "Optical hyperlens: far-field imaging beyond the diffraction limit," *Optics Express*, vol. 14, no. 18, pp. 8247–8256, 2006.

[14] Z. W. Liu, H. Lee, Y. Xiong, C. Sun, and X. Zhang, "Far-field optical hyperlens magnifying sub-diffraction-limited objects," *Science*, vol. 315, no. 5819, p. 1686, 2007.

[15] M. Huang and J. J. Yang, "Microwave sensor using metamaterials," in *Wave Propagation*, A. Petrin, Ed., pp. 13–36, InTech Inc., Klagenfurt, Austria, 2011.

[16] M. Schueler, C. Mandel, M. Puentes, and R. Jakoby, "Metamaterial inspired microwave sensors," *IEEE Microwave Magazine*, vol. 13, no. 2, pp. 57–68, 2012.

[17] T. Chen, S. Li, and H. Sun, "Metamaterials application in sensing," *Sensors*, vol. 12, no. 3, pp. 2742–2765, 2012.

[18] N. Wenwei, H. Ming, X. Zhe, and Y. Jingjing, "Sensitivity enhancement in optical waveguide sensors based on TM wave and metamaterials," in *Proceedings of the 9th International Symposium on Antennas Propagation and EM Theory (ISAPE '10)*, pp. 697–700, Guangzhou, China, November-December 2010.

[19] W. Niu, M. Huang, Z. Xiao, L. Zheng, and J. Yang, "Sensitivity enhancement in TE mode nonlinear planar optical waveguide sensor with metamaterial layer," *Optik*, 2011.

[20] W. Niu, M. Huang, Z. Xiao, and J. Yang, "Nonlinear planar optical waveguide sensor loaded with metamaterials," *Optoelectronics and Advanced Materials*, vol. 5, no. 10, pp. 1039–1045, 2011.

[21] J. J. Yang, M. Huang, J. Yu, and Y. Z. Lan, "Surface whispering-gallery mode," *Europhysics Letters*, vol. 96, no. 5, Article ID 57003, 2011.

[22] W. W. Niu, M. Huang, J. Sun, J. J. Yang, J. Yang, and J. Yu, "Microdisk sensor based on double negative metamaterials," *International Journal of RF and Microwave Computer-Aided Engineering*, vol. 22, no. 4, pp. 512–521, 2012.

[23] J. J. Yang, M. Huang, and J. Sun, "Double negative metamaterial sensor based on microring resonator," *IEEE Sensor Journal*, vol. 11, no. 10, pp. 2254–2259, 2011.

[24] M. Huang, J. Yang, S. Jun, S. Mu, and Y. Lan, "Simulation and analysis of a metamaterial sensor based on a microring resonator," *Sensors*, vol. 11, no. 6, pp. 5886–5899, 2011.

[25] M. Huang, J. Yang, J. Sun, J. Shi, and J. Peng, "Modelling and analysis of ω-shaped double negative material-assisted microwave sensor," *Journal of Infrared, Millimeter, and Terahertz Waves*, vol. 30, no. 11, pp. 1131–1138, 2009.

[26] J. J. Yang, M. Huang, Z. Xiao, and J. Peng, "Simulation and analysis of asymmetric metamaterial resonator-assisted microwave sensor," *Modern Physics Letters B*, vol. 24, no. 12, pp. 1207–1215, 2010.

[27] J. J. Yang, M. Huang, Y. Lan, and Y. Li, "Microwave sensor based on a single stereo-complementary asymmetric split resonator," *International Journal of RF and Microwave Computer-Aided Engineering*, vol. 22, no. 4, pp. 545–551, 2012.

[28] J. J. Yang, M. Huang, F. C. Mao, and Y. L. Li, "Experimental verification of a metamaterial open resonator," *Europhysics Letters*, vol. 97, no. 3, Article ID 37008, 2012.

[29] Z. Wu, M. Huang, J. Yang, J. Peng, and R. Zong, "Electromagnetic wave tunnelling and squeezing effects through 3D coaxial waveguide channel filled with ENZ material," in *Proceedings of the 8th International Symposium on Antennas, Propagation and EM Theory (ISAPE '08)*, pp. 550–553, Guangzhou, China, November 2008.

[30] N. I. Zheludev, "The road ahead for metamaterials," *Science*, vol. 328, no. 5978, pp. 582–583, 2010.

[31] K. Tiefenthaler and W. Lukosz, "Integrated optical switches and gas sensors," *Optics Letters*, vol. 9, no. 4, pp. 137–139, 1984.

[32] K. A. Remley and A. Weisshaar, "Design and analysis of a silicon-based antiresonant reflecting optical waveguide chemical sensor," *Optics Letters*, vol. 21, no. 16, pp. 1241–1243, 1996.

[33] R. Gravina, G. Testa, and R. Bernini, "Perfluorinated plastic optical fiber tapers for evanescent wave sensing," *Sensors*, vol. 9, no. 12, pp. 10423–10433, 2009.

[34] S. K. Khijwania and B. D. Gupta, "Maximum achievable sensitivity of the fiber optic evanescent field absorption sensor based on the U-shaped probe," *Optics Communications*, vol. 175, no. 1, pp. 135–137, 2000.

[35] C. Elosua, I. R. Matias, C. Bariain, and F. J. Arregui, "Volatile organic compound optical fiber sensors: a review," *Sensors*, vol. 6, no. 11, pp. 1440–1465, 2006.

[36] S. Guo and S. Albin, "Transmission property and evanescent wave absorption of cladded multimode fiber tapers," *Optics Express*, vol. 11, no. 3, pp. 215–223, 2003.

[37] A. Veselov, C. Thür, A. Efimov, M. Guina, H. Lemmetyinen, and N. Tkachenko, "Acidity sensor based on porphyrin self-assembled monolayers covalently attached to the surfaces of tapered fibres," *Measurement Science and Technology*, vol. 21, no. 11, Article ID 115205, 2010.

[38] M. Ahmad and L. L. Hench, "Effect of taper geometries and launch angle on evanescent wave penetration depth in optical fibers," *Biosensors and Bioelectronics*, vol. 20, no. 7, pp. 1312–1319, 2005.

[39] R. Horváth, H. C. Pedersen, and N. B. Larsen, "Demonstration of reverse symmetry waveguide sensing in aqueous solutions," *Applied Physics Letters*, vol. 81, no. 12, pp. 2166–2168, 2002.

[40] R. Horváth, L. R. Lindvold, and N. B. Larsen, "Reverse-symmetry waveguides: theory and fabrication," *Applied Physics B*, vol. 74, no. 4-5, pp. 383–393, 2002.

[41] S. A. Taya, M. M. Shabat, and H. M. Khalil, "Nonlinear planar asymmetrical optical waveguides for sensing applications," *Optik*, vol. 121, no. 9, pp. 860–865, 2010.

[42] S. A. Taya, M. M. Shabat, and H. M. Khalil, "Enhancement of sensitivity in optical waveguide sensors using left-handed materials," *Optik*, vol. 120, no. 10, pp. 504–508, 2009.

[43] Y. C. Lai, H. C. Lee, S. W. Kuo et al., "Label-free, coupler-free, scalable and intracellular bio-imaging by multimode plasmonic resonances in split-ring resonators," *Advanced Materials*, vol. 24, no. 23, pp. OP148–OP152, 2012.

[44] B. Reinhard, K. M. Schmitt, V. Wollrab, J. Neu, R. Beigang, and M. Rahm, "Metamaterial near-field sensor for deep-subwavelength thickness measurements and sensitive refractometry in the terahertz frequency range," *Applied Physics Letters*, vol. 100, no. 22, pp. 221101–221104, 2012.

[45] J. J. Yang, M. Huang, D. Z. Chen, H. W. Ding, and F. C. Mao, "Surface WGM sensor based on cylindrical dielectric waveguide," *Laser Physics Letters*, vol. 10, no. 1, Article ID 015901, 2012.

[46] G. Kenanakis, N. H. Shen, C. Mavidis et al., "Microwave and THz sensing using slab-pair-based metamaterials," *Physica B*, vol. 407, no. 20, pp. 4070–4074, 2012.

[47] J. F. O'Hara, R. Singh, I. Brener et al., "Thin-film sensing with planar terahertz metamaterials: sensitivity and limitations," *Optics Express*, vol. 16, no. 3, pp. 1786–1795, 2008.

[48] R. Melik, E. Unal, N. K. Perkgoz, C. Puttlitz, and H. V. Demir, "Metamaterial-based wireless strain sensors," *Applied Physics Letters*, vol. 95, no. 1, Article ID 011106, 2009.

[49] N. Papasimakis, Z. Luo, Z. X. Shen et al., "Graphene in a photonic metamaterial," *Optics Express*, vol. 18, no. 8, pp. 8353–8359, 2010.

[50] R. Melik, E. Unal, N. K. Perkgoz et al., "Nested metamaterials for wireless strain sensing," *IEEE Journal on Selected Topics in Quantum Electronics*, vol. 16, no. 2, pp. 450–458, 2010.

[51] N. Liu, T. Weiss, M. Mesch et al., "Planar metamaterial analogue of electromagnetically induced transparency for plasmonic sensing," *Nano Letters*, vol. 10, no. 4, pp. 1103–1107, 2010.

[52] M. Navarro-Cia, M. Aznabet, M. Beruete et al., "Stacked complementary metasurfaces for ultraslow microwave metamaterials," *Applied Physics Letters*, vol. 96, no. 16, pp. 164103–164103-3, 2010.

[53] N. Liu, L. Langguth, T. Weiss et al., "Plasmonic analogue of electromagnetically induced transparency at the Drude damping limit," *Nature Materials*, vol. 8, no. 9, pp. 758–762, 2009.

[54] B.-J. Seo, K. Kim, S. G. Kim, A. Kim, H. Cho, and E. Choi, "Observation of trapped-modes excited in double-layered symmetric electric ring resonators," *Journal of Applied Physics*, vol. 111, no. 11, Article ID 113106, 2012.

[55] N. R. Han, Z. C. Chen, C. S. Lim, B. Ng, and M. H. Hon, "Broadband multi-layer terahertz metamaterials fabrication and characterization on flexible substrates," *Optics Express*, vol. 19, no. 8, pp. 6990–6998, 2011.

[56] R. Aylo, P. P. Banerjee, A. K. Ghosh, and P. Verma, "Design of metamaterial based sensors for pressure measurement," in *Proceedings of the 9th International Symposium on Antennas Propagation and EM Theory (ISAPE '10)*, vol. 7604, pp. 760412–760412-8, San Francisco, Calif, USA, January 2010.

[57] D. Shreiber, M. Gupta, and R. Cravey, "Comparative study of 1-D and 2-D metamaterial lens for microwave nondestructive evaluation of dielectric materials," *Sensors and Actuators A*, vol. 165, no. 2, pp. 256–260, 2011.

[58] I. A. I. Al-Naib, C. Jansen, and M. Koch, "Thin-film sensing with planar asymmetric metamaterial resonators," *Applied Physics Letters*, vol. 93, no. 8, Article ID 083507, 2008.

[59] A. Alu and N. Engheta, "Dielectric sensing in epsilon-near-zero narrow waveguide channels," *Physical Review B*, vol. 78, no. 4, Article ID 045102, 2008.

[60] Z. Wei, Y. Cao, J. Han, C. Wu, Y. Fan, and H. Li, "Broadband negative refraction in stacked fishnet metamaterial," *Applied Physics Letters*, vol. 97, no. 14, Article ID 141901, 2010.

[61] C. P. Scarborough, Z. H. Jiang, D. H. Werner, C. Rivero-Baleine, and C. Drake, "Experimental demonstration of an isotropic metamaterial super lens with negative unity permeability at 8. 5 MHz," *Applied Physics Letters*, vol. 101, no. 1, Article ID 014101, 2012.

[62] K. Aydin, I. Bulu, and E. Ozbay, "Subwavelength resolution with a negative-index metamaterial superlens," *Applied Physics Letters*, vol. 90, no. 25, Article ID 254102, 2007.

[63] K. Y. Yang, V. Giannini, A. O. Bak, H. Amrania, S. A. Maier, and C. C. Phillips, "Subwavelength imaging with quantum metamaterials," *Physical Review B*, vol. 86, no. 7, Article ID 075309, 2012.

[64] V. A. Fedotov, M. Rose, S. L. Prosvirnin, N. Papasimakis, and N. I. Zheludev, "Sharp trapped-mode resonances in planar metamaterials with a broken structural symmetry," *Physical Review Letters*, vol. 99, no. 14, Article ID 147401, 2007.

[65] X. J. He, Y. Wang, J. M. Wang, and T. L. Gui, "Thin-film sensor based tip-shaped split ring resonator metamaterial for microwave application," *Microsystem Technologies*, vol. 16, no. 10, pp. 1735–1739, 2010.

[66] Z. Ren, M. S. Boybay, and O. M. Ramahi, "Near-field subsurface detection using metamaterial inspired probes," *Applied Physics A*, vol. 103, no. 3, pp. 839–842, 2011.

[67] M. S. Boybay and O. M. Ramahi, "Near-field probes using double and single negative media," *Physical Review E*, vol. 79, no. 1, Article ID 016602, 2009.

[68] A. Penirschke, M. Schussler, and R. Jakoby, "New microwave flow sensor based on a left-handed transmission line resonator," in *Proceedings of the IEEE MTT-S International Microwave Symposium (IMS '07)*, pp. 393–396, June 2007.

[69] M. Schussler, M. Puentes, C. Mandel, and R. Jakoby, "Capacitive level sensor for layered fillings in tanks and vessles based on metamaterial transmission line," in *Proceedings of IEEE Sensors*, pp. 1966–1969, 2011.

[70] M. Puentes, M. Schüler, C. Damm, and R. Jakoby, "Extraction of capacitive profiles with a planar metamaterial sensor," *Applied Physics A*, vol. 103, no. 3, pp. 815–819, 2011.

[71] C. Mandel, M. Schussler, and R. Jakoby, "A wireless passive strain sensor," in *Proceedings of IEEE Sensors*, pp. 207–210, 2011.

[72] M. Puentes, B. Stelling, M. Schüßler, A. Penirschke, and R. Jakoby, "Planar sensor for permittivity and velocity detection based on metamaterial transmission line resonator," in *Proceedings of the 39th European Microwave Conference (EuMW '09)*, pp. 57–60, October 2009.

[73] M. Notomi, "Theory of light propagation in strongly modulated photonic crystals: refractionlike behavior in the vicinity of the photonic band gap," *Physical Review B*, vol. 62, no. 16, pp. 10696–10705, 2000.

[74] S. L. He, Y. Jin, Z. C. Ruan, and J. G. Kuang, "On subwavelength and open resonators involving metamaterials of negative refraction index," *New Journal of Physics*, vol. 7, no. 1, p. 210, 2005.

[75] M. Silveirinha and N. Engheta, "Tunneling of electromagnetic energy through subwavelength channels and bends using ε-near-zero materials," *Physical Review Letters*, vol. 97, no. 15, pp. 157–403, 2006.

[76] B. Edwards, A. Alù, M. E. Young, M. Silveirinha, and N. Engheta, "Experimental verification of epsilon-near-zero metamaterial coupling and energy squeezing using a microwave waveguide," *Physical Review Letters*, vol. 100, no. 3, Article ID 033903, 2008.

[77] A. Alù and N. Engheta, "Light squeezing through arbitrarily shaped plasmonic channels and sharp bends," *Physical Review B*, vol. 78, no. 3, Article ID 035440, 2008.